15 June 2000

ELSEVIER

Optics Communications 180 (2000) 301–315

OPTICS COMMUNICATIONS

www.elsevier.com/locate/optcom

Experimental and theoretical studies of a high repetition rate fiber laser, mode-locked by external optical modulation

K. Zoiros, T. Stathopoulos, K. Vlachos, A. Hatziefremidis, T. Houbavlis, T. Papakyriakopoulos, H. Avramopoulos *

National Technical University of Athens, Department of Electrical and Computer Engineering, Photonics Communications Research Laboratory, 9 Iroon Polytechniou Street, 15773 Zografou, Athens, Greece

Received 2 December 1999; received in revised form 28 March 2000; accepted 11 April 2000

Abstract

An experimental and theoretical study of a high repetition rate laser source operating on a novel mode-locking technique is presented. This technique relies on the fast saturation and recovery of a semiconductor optical amplifier induced by an external optical pulse and has been used to obtain 4.3 ps pulses at 20 GHz. A complete mathematical model of the fiber ring laser is presented describing the mode-locking process in the laser oscillator and providing solutions for the steady-state mode-locked pulse profile. The critical parameters of the system are defined and analyzed and their impact on the formation of the mode-locked pulses is examined. The comparison between the theoretical results and the experimental data reveals very good agreement and has allowed the optimization of the performance of the system in terms of its critical parameters.

PACS: 42.55.Px; 42.60.Fc
Keywords: Active mode-locking; High repetition rate ring laser; Semiconductor optical amplifier; External optical modulation

1. Introduction

Ultra-high speed optical communications networks are evolving rapidly and are being deployed to satisfy the increasing bandwidth demand due to the massive use of Internet, multimedia and other bandwidth hungry applications. Optical signal sources capable of generating ultra-short pulse trains at high repetition rates [1] are key elements for these novel photonic networks that may combine wavelength division multiplexing (WDM) and optical time domain multiplexing (OTDM) transmission techniques [2]. Short pulse, high repetition rate lasers are also essential for ultra-high speed, all-optical logic experiments [3–5]. Active mode-locking is one of the main methods for the generation of ultra-short transform-limited optical pulses and is achieved by direct modulation of the optical field during each cavity round-trip. This method is particularly important especially when synchronization between optical and electrical signals is required. At 1.5 μm, several actively mode-locked fiber lasers employing erbium-doped fiber as the gain medium and produc-

* Corresponding author. Tel.: +30-1-772-2076; fax: +30-1-772-2077; e-mail: hav@cc.ece.ntua.gr

0030-4018/00/$ - see front matter
PII: S0030-4018(00)00708-2

ing transform-limited picosecond pulses at multi-GHz rates have been demonstrated [6–16]. The majority of these systems uses loss modulation by lithium niobate electro-optic modulators due to their large electro-optic coefficient and their compact construction on low loss titanium-undiffused waveguides. Unfortunately, lithium niobate modulators tend to display sensitivity on the polarization state of the input optical field. As a result of this sensitivity, laser sources using lithium niobate modulators either have to be build from polarization preserving fiber pigtailed components [10–12] or else suffer from mode-locking loss which limits their operational usability. Similarly, the use of lightly or moderately doped Er fiber for gain results in long cavities which make fiber lasers sensitive to small environmental perturbations, such as thermal fluctuations and acoustic vibration. Active stabilization techniques have been developed to counter the tendency towards instability of long cavity fiber lasers but at the price of added system complexity [13–16]. In order to solve these problems, semiconductor optical amplifiers (SOAs) have been deployed in mode-locked laser sources for the generation of short optical pulses at high repetition rates as they can provide gain over a broad spectral range as well as modulation due to their fast gain dynamics. Specifically, actively mode-locked laser sources incorporating an SOA have been demonstrated by several research groups [17–30] to generate short optical pulses at various repetition rates. In these configurations the role of the SOA is to provide either the necessary gain exceeding the ring laser cavity loss in combination with an intracavity electroabsorption [17,18] or electro-optic modulator [19,20] or to provide both gain and electrically controlled gain modulation [21–30]. SOAs have been also used as the mode-locking elements providing gain modulation in Er-doped fiber ring lasers that generate ultra-high speed trains of picosecond pulses [31] as well as in high rate all-optical pulse storage rings [32] based on cross-gain saturation.

This paper presents experimental and theoretical studies on an actively mode-locked fiber ring laser that uses a single SOA to provide both gain and gain modulation using cross gain saturation from an external optical pulse train [33]. The source is very simple to build from commercially available components and produces nearly transform-limited 4.3 ps pulses at 10 and 20 GHz over 16 nm tuning range. This configuration results in a stable oscillator since the use of a single active element to provide both gain and modulation renders the cavity short. Furthermore, the cavity is nearly polarization insensitive as there is no lithium niobate modulator and the SOA is operated under heavy saturation providing nearly polarization-independent gain. One consequence of using a cavity with a single active, optically modulated SOA, is its ability to produce mode-locked pulses at a harmonic repetition frequency of the external signal. This can be achieved by tuning the frequency, f_{ext}, of the externally introduced pulse train to $f_{ext} = (N + 1/n)f_{ring}$, where N is the order of harmonic mode-locking of the ring laser, f_{ring} is the fundamental frequency of the ring laser oscillator and n is an integer number greater than 1, to obtain an output pulse train at the frequency nf_{ext}. Repetition frequency multiplication by fractional harmonic mode-locking has been used in mode-locked laser diodes [34], all-optical storage loops [35] and external cavity semiconductor lasers [36]. Fractional harmonic mode-locking has also been used with the source described here and has provided up to 40 GHz repetition rate pulse trains [37,38].

A mathematical model of the fiber ring laser is presented describing the mode-locking process in the laser oscillator and providing solutions for the steady-state mode-locked pulse profile. The model enables the prediction of the duration of the mode-locked pulse that exits the fiber ring laser source versus the duration of the external pulse that is inserted in the system. A complete investigation on the critical parameters that determine the width, energy and position of the mode-locked pulse relative to the external pulse has been performed. These parameters include the small signal gain and carrier lifetime of the SOA, the cavity loss and the pulse energy and width of the external modulating signal. It has been found both experimentally and theoretically that the minimum pulse width is obtained when these parameters are adjusted so that the mode-locked pulse forms midway between two successive external pulses and that this condition corresponds to the case where the energies of the external and mode-locked pulses are nearly equal. A rule of thumb is also given concerning the relationship between the

operating repetition period and the carrier lifetime of the SOA which is particularly important when the fiber ring laser source is used for ultra-high speed all-optical applications.

The remainder of this paper is organized as follows. Section 2 presents the experimental results of the fiber ring source. Section 3 is devoted to the development of the theoretical model describing the mode-locking process. Section 4 presents the theoretical results obtained from the model and provides detailed comparison with the experimental data as well as design guidelines for the extension of the operation of this source. Finally, Section 5 contains the conclusion.

2. Experimental results of mode-locking by externally introduced optical pulse

Fig. 1 shows the experimental layout. The laser ring cavity was constructed from standard fiber pigtailed components. Gain was provided from a bulk InGaAsP/InP ridge waveguide SOA. The device has ridge width of 3 μm, the active layer thickness of 240 nm and length of 500 μm and has been mounted p-side up on a copper submount. In order to reduce the facet reflectivity the waveguide is 10° tilted with respect to the output facets and a two layer antireflection coating (SiO/Al_2O_3) has been evaporated on the chip facets. The SOA structure has a high confinement factor for the TE mode of about 0.4 resulting in high chip gain. The device provides 23 dB small signal gain at 1535 nm with 400 mA drive current and has 400 ps recovery time. In order to ensure unidirectional oscillation in the ring and to stop the externally introduced signal from circulating in the cavity, Faraday isolators were used at the input and output of the SOA. A 3 dB fiber coupler was placed just after SOA for the insertion of the external pulsed signal as well as for output extraction. A tunable filter with 5 nm bandwidth was employed to perform wavelength selection. The SOA exhibited a 2 dB polarization dependence at small signal and this was further reduced under saturation conditions. In order to optimize the performance of the source, a polarization controller was introduced at its input port. This controller was adjusted at the beginning of the session and required no further adjustment during operation. The total length of the ring cavity was 14.5 m corresponding to a 13.79 MHz fundamental frequency which could be significantly reduced. The externally introduced pulses were generated from a 10 GHz gain switched DFB diode laser operating at 1548.5 nm. The 10 GHz pulse trains could be passed through an optional repetition frequency fiber doubler to generate a 20 GHz external pulse signal. The pulses were compressed to 8 ps using a dispersion compensating fiber and were amplified in an EDFA before launching into the ring cavity. A polarization controller was used to control the polarization state of the gain switched pulses before entry into the ring and again adjustment was only required at the beginning of a session for best mode-locked performance. With the DFB laser diode gain switched at around 10 GHz, the frequency micro-adjusted to be a harmonic of the fiber ring oscillator and the EDFA adjusted to provide 400 μW average power in the ring cavity, the ring laser source breaks into stable, mode-locked operation. The use of the optional repetition frequency doubler on the gain switched pulses to produce a 20 GHz pulse train in combination with an increase of the power provided from the EDFA into the fiber ring cavity to 500 μW, causes the laser to mode-lock at 20 GHz. Fig. 2(a) shows the mode-locked pulse train at 20 GHz monitored on an optical

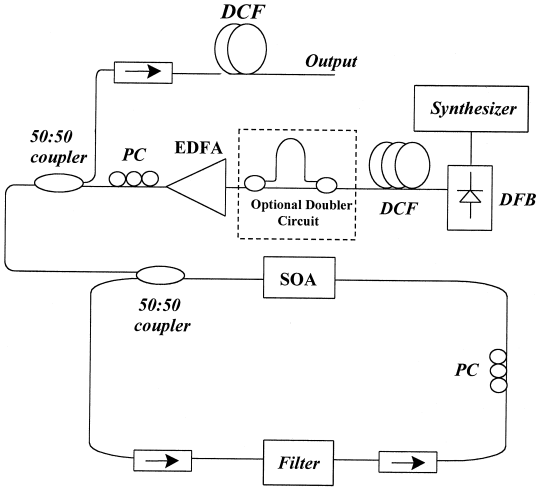

Fig. 1. Experimental layout. DFB, distributed feedback laser; DCF, dispersion compensating fiber; EDFA, Er-doped fiber amplifier; PC, polarization controller; SOA, semiconductor optical amplifier.

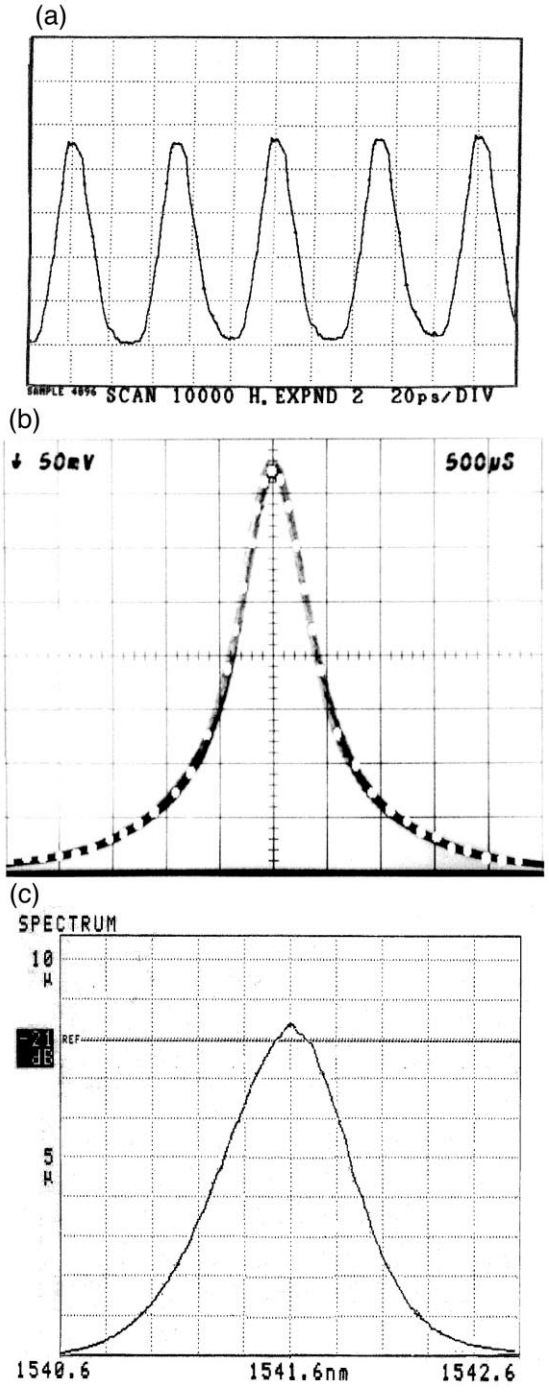

Fig. 2. (a) 20 GHz optical pulse train. (b) Second harmonic autocorrelation trace obtained at 20 GHz showing a 4.3 ps pulse assuming a hyperbolic secant profile. The time base corresponds to 4.15 ps. (c) Optical spectrum of mode-locked pulses.

sampling oscilloscope (Hamamatsu-OOS-01). The output pulses were also monitored on a second harmonic autocorrelator and were found to be non transform-limited with 8 ps deconvolved duration at either repetition rate. The extra frequency chirp resulting primarily from the saturation of the SOA was compensated at the output of the laser with a dispersion compensating fiber of -11.4 ps per nm dispersion. Fig. 2(b) shows the autocorrelation trace of the pulse train at 20 GHz obtained at 1541.6 nm. The trace has been fitted with the autocorrelation of a squared hyperbolic secant profile of 4.3 ps pulse width (white dots) and shows a good fit. Pulse-to-pulse timing jitter was measured to be less than 500 fs at 20 GHz. Fig. 2(c) shows the corresponding optical spectrum. The indicated pulse width–bandwidth product of the output is 0.34 and is very close to that of a transform-limited squared hyperbolic secant profile. Fig. 3 shows the change of the pulse width and the average optical power of the mode-locked source versus wavelength when operated at 20 GHz, indicating nearly constant pulse width across its 16 nm tuning range. Similar results were acquired when the source was mode-locked at 10 GHz.

The precise pulse formation in the oscillator relies on the way the SOA is saturated by the external and mode-locked pulses that enter it. In order to investigate the mode-locking process, the dependence of the position of the mode-locked pulse relative to the external pulse has been examined with respect to the energy of the external pulse. The timing measure-

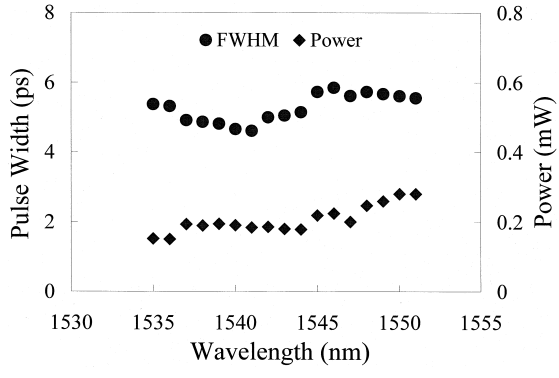

Fig. 3. Tuning curve for pulse width, FWHM, and average power of mode-locked pulses at 20 GHz.

ments of the external pulse were performed on the ASE signal emerging from the cavity with the oscillation blocked. Fig. 4 shows the variation of the width of the mode-locked pulses and the relative time delay between the external and mode-locked pulses with respect to the energy of the external pulse when the oscillator operates at 10 GHz. This figure shows that the minimum pulse width was obtained when the mode-locked pulse forms midway between two successive external pulses. In this case, the energy of the external pulse injected inside the cavity was about 40 fJ and similar in value to the energy of the recirculating mode-locked pulse.

The sensitivity of the oscillator on the polarization state of the recirculating mode-locked signal and the external pulse train was also examined by adjustment of the cavity and external polarization controllers. It was found that there was up to 25% pulse broadening and up to 20% power decrease in the output pulse train with the controllers adjusted furthest from their optimum location but there was no pulse train loss. In order to examine the sensitivity of the oscillator to temperature variations, the RF bandwidth over which the ring oscillator mode-locks as the repetition frequency of the external pulse train is varied was also measured. This was found to be 400 KHz, corresponding to 2.7 ps variation in the roundtrip time of the ring cavity. By comparison, the differential time delay in the cavity roundtrip time due to the temperature dependence of the refractive index in the core of the fiber is only 0.6 ps, with a 2°C temperature variation and assuming a 20 ps/km°C temperature-dependent differential delay

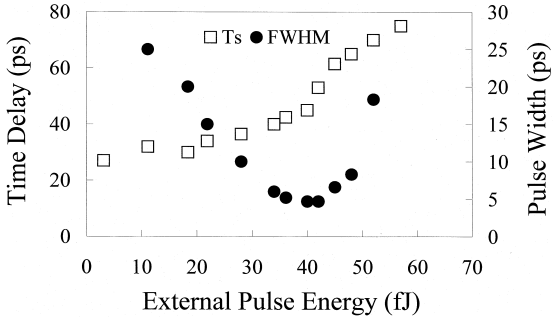

Fig. 4. Pulse width, FWHM, and relative time delay of the mode-locked and external pulses, T_s, against external pulse energy at 10 GHz.

coefficient for the fiber. These quantitative measurements verified the operational experience regarding the stability of the laser source. Once set, the system was stable, requiring no further adjustments and there was no appreciable degradation of its performance over several hours.

3. Model for mode-locking using optical gain modulation of a semiconductor optical amplifier

Mode-locking is a well established technique for the generation of ultra-short pulses and has been investigated theoretically by several research groups [39–43]. Especially, active mode-locking has received considerable theoretical interest that has included analytical [44–46] and numerical treatment [27,47–50] for the estimation of mode-locked pulse characteristics.

This section presents the mathematical model that describes the mode-locking process of the SOA fiber ring cavity. The model is based on the self-reproducing pulse profile model that was originally developed by Haus [41] and which has been modified to describe active mode-locking based on the saturation of the gain of an SOA from an external optical pulse train. The model follows the unidirectional propagation of the pulse around the laser cavity. The operations that have been considered are: (a) saturable gain in the semiconductor optical amplifier by the externally introduced pulse and the circulating mode-locked pulse, (b) bandwidth limitation of the circulating pulse with an optical filter, and (c) linear losses.

The parameters of the model are assumed to possess values for which the oscillator operates under steady-state mode-locked condition. The pulse is therefore assumed to reproduce itself after one complete circulation around the laser cavity without any changes in the width or the energy, apart from a small temporal displacement. The other implicit assumptions which have been made in order to obtain the solutions are as follows: (a) the electric field of the circulating mode-locked pulse is assumed to be linearly polarized along the SOA axis of peak gain; (b) changes in the mode-locked pulse profile due to

its transit through each cavity element are small; as such, Taylor expansions of exponential terms to the first order incur small errors in the analysis; (c) the pulse energy of the external optical pulse and the circulating mode-locked pulse is assumed to be low enough compared to the saturation energy of the SOA; as a result of this, the gain coefficient of the SOA may be expanded up to second order with respect to pulse energies; (d) the bandwidth of the mode-locked pulse is assumed to be small compared to the bandwidth of the spectral limiting element in the cavity and Taylor expansion to second order of the pulse spectrum in the frequency domain is appropriate.

3.1. Steady-state equations

The modification of the optical pulse after the consecutive transit through the SOA, spectral filter and after encountering the cavity linear losses, may be found by successive operation of three operators $\hat{O}_1$, $\hat{O}_2$ and $\hat{O}_3$ on the input pulse profile $E_{in}(t)$.

$\hat{O}_1$ is defined as the gain operator of the SOA acting on the electric field of the input pulses

$$\hat{O}_1 \equiv \exp\left[\frac{G(t)}{2}\right]$$

where $G(t)$ is the time-dependent power gain coefficient of the SOA.

$\hat{O}_2$ is defined as the time domain transfer operator of the pulse through the filter

$$\hat{O}_2 \equiv \exp\left[\frac{1}{2\,\Delta\omega_c}\frac{d^2}{dt^2}\right]$$

where $\Delta\omega_c$ is related to the full width at half maximum, $\Delta\omega_f$, of the filter transfer function by

$$\Delta\omega_c = \frac{1}{2\sqrt{\ln 2}}\Delta\omega_f \tag{1}$$

Finally, $\hat{O}_3$ is defined as the linear loss operator

$$\hat{O}_3 \equiv \exp\left[-\frac{L}{2}\right]$$

where L is the power linear loss coefficient of the system. The output pulse is thus

$$\begin{aligned} E_{out}(t) &= \hat{O}_1\hat{O}_2\hat{O}_3[E_{in}(t)] \\ &= \exp\left[-\frac{L}{2}\right]\exp\left[\left(\frac{1}{2\Delta\omega_c^2}\frac{d^2}{dt^2}\right)\right] \\ &\quad\times\exp\left[\frac{G(t)}{2}\right]E_{in}(t-T_1-T_2-T_3) \end{aligned} \tag{2}$$

where T_1 is the transit time of the pulse through the SOA, T_2 is the temporal delay that the pulse experiences when travelling from the exit of the SOA to the exit of the filter, and T_3 is the temporal delay that the pulse experiences to travel from the exit of the filter to the entrance of the SOA.

On the assumption that the profile change per pulse transit is small, the exponential terms in Eq. (2) may be expanded to first order providing

$$\begin{aligned} E_{out}(t) &= \left[1-\frac{L}{2}+\left(\frac{1}{2\,\Delta\omega_c^2}\frac{d^2}{dt^2}+\frac{G(t)}{2}\right)\right] \\ &\quad\times E_{in}(t-T_R) \end{aligned} \tag{3}$$

where $T_R = T_1 + T_2 + T_3$ is the round trip time of the laser cavity, which for simplicity is assumed to be equal to the repetition period, T_{ext}, of the externally introduced pulse train. In practice, such a laser system would be harmonically mode-locked so that $T_R = mT_{ext}$, where m is an integer.

In order to obtain closure and a steady-state solution for the mode-locked pulse, the mode-locked pulse is assumed to reproduce itself after each complete transit through the SOA, filter and losses. The gain of the SOA is also assumed to recover to the same value before each mode-locked pulse enters it. In order to accommodate small temporal shifts, δT, of the pulse around its peak as a result of the gain saturation in the SOA, the self-reproducing pulse profile principle is applied by requiring that

$$E_{out}(t) = E_{in}(t - T_R + \delta T) \tag{4}$$

and by expanding to first order in δT we obtain

$$\delta T \frac{\mathrm{d}E_{\mathrm{in}}}{\mathrm{d}t} = -\frac{L}{2}\left[1 - \frac{1}{L}\frac{1}{\Delta\omega_{\mathrm{c}}^2}\frac{\mathrm{d}^2}{\mathrm{d}t^2} - \frac{G(t)}{L}\right]E_{\mathrm{in}}(t) \tag{5}$$

Introducing the normalized parameters

$$\delta = \frac{2}{L}\Delta\omega_{\mathrm{c}}\,\delta T \tag{6}$$

and

$$g(t) = \frac{G(t)}{L} \tag{7}$$

where $g(t)$ is the gain coefficient of the SOA normalized to the linear loss coefficient, and δ is a time delay (or advance) parameter indicating whether the pulse repetition period deviates from the free space round trip time, T_{R}, Eq. (5) becomes

$$\left[1 - g(t) - \frac{1}{L}\frac{1}{\Delta\omega_{\mathrm{c}}^2}\frac{\mathrm{d}^2}{\mathrm{d}t^2} + \frac{\delta}{\Delta\omega_{\mathrm{c}}}\frac{\mathrm{d}}{\mathrm{d}t}\right]E_{\mathrm{in}}(t) = 0 \tag{8}$$

The solution of this steady-state equation for the recirculating mode-locked pulse requires the calculation of the time-dependent normalized gain coefficient $g(t)$. For this purpose, we consider in Section 3.2 the gain dynamics of the SOA during its gain saturation and recovery periods. In the analysis that follows, it is assumed that the external pulses are temporally separated from the mode-locked pulses by an unknown parameter, T_{s}. Fig. 4 shows that the external and mode-locked pulses are well separated from each other in the experiment so that T_{s} can be assumed to be large compared to the width of the two pulses. Physically, this means that the external pulse energy does not play any direct role in saturating the gain of the SOA during the presence of the mode-locked pulse and therefore need not be taken into account in Eq. (8) explicitly. The effect of the saturation of the SOA by the external pulses is, however, taken into account in calculating the input gain parameter at the entrance point of the mode-locked pulses as will be described in Section 3.2.2.

3.2. Semiconductor optical amplifier gain dynamics

The gain coefficient inside the SOA displays a temporal and spatial dependence governed by the rate equations of the carrier density at a specific coordinate z in the amplifier at time t, $N(z,t)$. It is convenient to define the integrated time-dependent power gain coefficient of the SOA, $G(t)$, along its length, ℓ, which takes implicitly into account the spatial variation of the gain coefficient and corresponds to the gain coefficient measured experimentally. This is given by

$$G(t) = \int_0^{\ell} G(z,t)\,\mathrm{d}z \tag{9}$$

The ordinary differential equation that governs the temporal saturation of the integrated gain coefficient $G(t)$ for each point in the pulse is [51]

$$\frac{\mathrm{d}G(t)}{\mathrm{d}t} = \frac{G_{\mathrm{ss}} - G(t)}{t_{\mathrm{car}}} - \frac{cn\varepsilon_0 A}{2}\frac{|E_{\mathrm{in}}(t)|^2}{J_{\mathrm{sat}}} \times \left(\exp\left[G(t)\right] - 1\right) \tag{10}$$

where G_{ss} is the integrated small signal gain coefficient, t_{car} is the carrier lifetime, c is the speed of light in vacuum, n is the index of refraction, ε_0 is the dielectric constant in vacuum, A is the cross-section area of the active region, and J_{sat} is the saturation energy of the amplifier

$$J_{\mathrm{sat}} = \hbar\omega_0 A/\sigma \tag{11}$$

where $\hbar\omega_0$ is the photon energy, and σ is the transition cross-section. The term $|E_{\mathrm{in}}(t)|^2$ is proportional to the inserted optical power of the recirculating mode-locked pulses in the SOA.

Assuming for simplicity that around the peak of the mode-locked pulse $G(t)$ is close to 1 so that the exponential term in (10) may be expanded to first order and by dividing both sides of the equation with the cavity linear loss, L, the following differential

equation that describes the gain dynamics of the SOA is obtained from (7) and (10)

$$\frac{\mathrm{d}\, g(t)}{\mathrm{d}t} = \frac{g_{ss} - g(t)}{t_{car}} - \frac{cn\varepsilon_0 A}{2} \frac{g(t)\,|E_{in}(t)|^2}{J_{sat}} \tag{12}$$

where g_{ss} is the integrated small signal gain normalized to the cavity linear losses

$$g_{ss} = G_{ss}/L = \Gamma\sigma N_0(I/I_0 - 1)/L \tag{13}$$

In this equation, Γ is the confinement factor, and N_0 and I_0 are the carrier density and injection current required for transparency, respectively.

3.2.1. Gain saturation by a short optical pulse

Eq. (12) can be now used to obtain the gain saturation of the SOA for a short optical pulse, on the assumption that the width of the pulse is much smaller than the carrier lifetime of the amplifier [51]. This in practice means that the optical pulse is so short that the gain has no time to recover during its duration and the first term in the right hand side of Eq. (12) can be thus neglected. The resulting normalized time-dependent gain $g(t)$ is

$$g(t) = g_{in}^{p} \exp\left[- \frac{J_{in}(t)}{J_{sat}} \right] \tag{14}$$

where g_{in}^{p} is the gain before the arrival of the recirculating mode-locked optical pulses, and

$$J_{in}(t) = \frac{cn\varepsilon_0 A}{2} \int_{-\infty}^{t} |E_{in}(t')|^2 \,\mathrm{d}t' \tag{15}$$

is the instantaneous energy of the mode-locked pulses entering the SOA. The exponential of (14) may be expanded, according to the assumptions already stated, into second-order Taylor series; substituting in (8) yields

$$\left[1 - g_{in}^{p} + g_{in}^{p} \frac{J_{in}(t)}{J_{sat}} - \frac{g_{in}^{p}}{2} \left(\frac{J_{in}(t)}{J_{sat}} \right)^2 \right] E_{in}(t) + \frac{\delta}{\Delta\omega_c} \frac{\mathrm{d}\, E_{in}(t)}{\mathrm{d}t} - \frac{1}{L} \frac{1}{\Delta\omega_c^2} \frac{\mathrm{d}^2 E_{in}(t)}{\mathrm{d}t^2} = 0 \tag{16}$$

The solution of this equation requires the knowledge of g_{in}^{p} which can be found from the gain recovery analysis that follows.

3.2.2. Gain recovery

After the saturation of the SOA according to (14), the gain recovers due to the injection of carriers by the injection current. The gain recovery can be calculated assuming that the stimulated recombination term (second term) in the right hand side of (12) can be neglected, from

$$\frac{\mathrm{d}\, g(t)}{\mathrm{d}t} = \frac{g_{ss} - g(t)}{t_{car}} \tag{17}$$

with solution

$$g(t) = (g_f - g_{ss}) \exp\left[- \frac{t}{t_{car}} \right] + g_{ss} \tag{18}$$

where g_f is the gain of the saturated SOA immediately after the transit of a pulse through given by

$$g_f = g_{in} \exp\left[- \frac{J_{total}}{J_{sat}} \right] \tag{19}$$

In this equation g_{in} and J_{total} are the SOA gain and pulse energy immediately before the pulse entrance into the SOA. Given that two different sets of pulses transit the SOA at different times, namely the external pulses and the mode-locked pulses, the recovery of the SOA must be accounted separately for these sets of pulses. For this reason, g_{in} takes in (19) the values g_{in}^{p} and g_{in}^{ext}, and J_{total} takes the values J_p and J_{ext} for the mode-locked and external pulses, respectively.

In order to obtain the steady-state condition for the laser oscillator, the gain of the SOA is assumed to recover always to the same level g_{in}^{p} and g_{in}^{ext} before the mode-locked and the external pulses enter it, respectively. As the mode-locked pulse forms at time T_s after the external pulse has entered the SOA, its gain has had $T_s - \Delta T$ time to recover to the value g_{in}^{p} from the value g_f^{ext} before the arrival of the mode-locked pulse, where $\Delta T = \frac{1}{2}(t_{ext} + t_p)$, with t_{ext} being the FWHM of the external pulses and t_p the width of the mode-locked pulses related to the FWHM according to Eq. (24). Similarly, the external pulse experiences a gain equal to g_{in}^{ext} which has recovered from the saturated value g_f^{p} after the mode-locked pulse exits the SOA after $T_R - T_s - \Delta T$ time has elapsed. The equation of the recovery of the SOA is thus separated in two equations which de-

scribe the SOA recovery after the transition of the external and mode-locked pulses, respectively. Eqs. (18) and (19) yield

$$g_{\mathrm{in}}^{\mathrm{p}} = \left[g_{\mathrm{in}}^{\mathrm{ext}} \exp\left(-\frac{J_{\mathrm{ext}}}{J_{\mathrm{sat}}} \right) - g_{\mathrm{ss}} \right] \times \exp\left[-\frac{T_{\mathrm{s}} - \Delta T}{t_{\mathrm{car}}} \right] + g_{\mathrm{ss}} \tag{20}$$

and

$$g_{\mathrm{in}}^{\mathrm{ext}} = \left[g_{\mathrm{in}}^{\mathrm{p}} \exp\left(-\frac{J_0}{J_{\mathrm{sat}}} \right) - g_{\mathrm{ss}} \right] \times \exp\left[-\frac{T_{\mathrm{R}} - T_{\mathrm{s}} - \Delta T}{t_{\mathrm{car}}} \right] + g_{\mathrm{ss}} \tag{21}$$

Substituting (21) in (20), $g_{\mathrm{in}}^{\mathrm{ext}}$ is eliminated and an expression is obtained which involves only $g_{\mathrm{in}}^{\mathrm{p}}$

$$g_{\mathrm{in}}^{\mathrm{p}} = \frac{g_{\mathrm{ss}}[1 + \exp(A - \alpha) - \exp(A + B - \alpha) - \exp(A)]}{[1 - \exp(A + B - U_0 - \alpha)]} \tag{22}$$

where $U_0 = (J_{\mathrm{p}}/J_{\mathrm{sat}})$ and $\alpha = (J_{\mathrm{ext}}/J_{\mathrm{sat}})$ are the normalized to the SOA saturation energy energies of the mode-locked and external pulses, respectively, $A = -(T_{\mathrm{s}} - \Delta T)/t_{\mathrm{car}}$ and $B = -(T_{\mathrm{R}} - T_{\mathrm{s}} - \Delta T)/t_{\mathrm{car}}$.

3.3. Solution

In order to obtain a steady-state solution for the mode-locked pulse profile in terms of its width and energy, the mode-locked pulses are assumed to be squared hyperbolic secant in shape with total energy J_{p} so that the electric field is given by

$$E_{\mathrm{in}}(t) = \left(\frac{U_0 J_{\mathrm{sat}}}{2 t_{\mathrm{p}}} \right)^{1/2} \operatorname{sech} \frac{t}{t_{\mathrm{p}}} \tag{23}$$

where t_{p} is related to the full width at half maximum, T_{FWHM}, by

$$t_{\mathrm{p}} = \frac{T_{\mathrm{FWHM}}}{\ln(3 + 2\sqrt{2})} \tag{24}$$

Squaring (23) and integrating over the time-dependent variable we obtain

$$\frac{J_{\mathrm{in}}(t)}{J_{\mathrm{sat}}} = \frac{U_0}{2} \left(1 + \tanh \frac{t}{t_{\mathrm{p}}} \right) \tag{25}$$

Substituting (23) and (25) and equating the coefficients of the same order terms in (16), the following equations are derived

$$1 - g_{\mathrm{in}}^{\mathrm{p}} + \frac{g_{\mathrm{in}}^{\mathrm{p}}}{2} - \frac{U_0^2}{8} - \frac{1}{L} \frac{1}{t_{\mathrm{p}}^2 \Delta \omega_{\mathrm{c}}^2} = 0 \tag{26}$$

$$\frac{g_{\mathrm{in}}^{\mathrm{p}} U_0}{2} - \frac{g_{\mathrm{in}}^{\mathrm{p}} U_0^2}{4} - \frac{\delta}{t_{\mathrm{p}} \Delta \omega_{\mathrm{c}}} = 0 \tag{27}$$

$$\frac{2}{L t_{\mathrm{p}}^2 \Delta \omega_{\mathrm{c}}^2} - \frac{g_{\mathrm{in}}^{\mathrm{p}} U_0^2}{8} = 0 \tag{28}$$

Eqs. (22), (26)–(28) form a set of nonlinear equations with unknowns, t_{p}, U_0, $g_{\mathrm{in}}^{\mathrm{p}}$ and δ. Setting

$$\delta = \frac{x}{L t_{\mathrm{p}} \Delta \omega_{\mathrm{c}}}$$

we obtain

$$g_{\mathrm{in}}^{\mathrm{p}} = \frac{(x+4)^2}{(x+4)^2 - 4(x+1)} \tag{29}$$

$$U_0 = \frac{8}{x+4} \tag{30}$$

and

$$t_{\mathrm{p}} \Delta \omega_{\mathrm{c}} = \frac{|x+4|}{2\sqrt{g_{\mathrm{in}}^{\mathrm{p}} L}}, \tag{31}$$

which is the desired final equation for the calculation of $t_{\mathrm{p}} \Delta \omega_{\mathrm{c}}$.

4. Results of the self-consistent model and discussion

4.1. Calculation of T_{TFWHM} $\Delta \omega_{\mathrm{f}}$

The calculation of $t_{\mathrm{p}} \Delta \omega_{\mathrm{c}}$ and U_0 is achieved by setting Eq. (22) equal to (29) and substituting for the known values of the period and pulse width of the external pulse train, the SOA carrier lifetime and the cavity loss. The derived equation in x is, however, transcendental and requires numerical solution. In order to solve the transcendental equation and find the unknown x, the parameters α and T_{s} are scanned in accordance with the current experimental conditions for a given value of the normalized small signal gain, g_{ss}, which is the only independent variable of

the nonlinear system of equations. The unknown x is also scanned within a range whose lower limit is determined by the fact that the normalized energy of the mode-locked pulses must be always less than the normalized energy of the external pulses. It is important to note that due to the form of the transcendental equation, the same combinations of the values of U_0 and α may correspond to multiple solutions of x. The selection of the single x solution and the elimination of the others is performed by choosing the value that yields the smallest pulse width. Therefore, by solving the system for minimum pulse width, the optimum value of T_s and α is obtained for the given g_{ss}. The value of x that corresponds to this set of g_{ss}, α and T_s, is then replaced in (31) to calculate $t_p \Delta\omega_c$ and the desired value of $T_{FWHM} \Delta\omega_f$ is finally obtained from (1) and (24).

4.2. Simulation results and discussion

Simulation results were obtained for repetition frequencies at 10 GHz and 20 GHz in order to compare them to the experimental ones. The parameters used for the simulations were chosen to agree with the values in the experimental configuration. Specifically, the width of the external pulses was 8 ps, the cavity loss was 15 dB and the full width at half maximum of the spectral limiting filter was 5 nm for both frequencies. The value of the carrier lifetime depends on the type of SOA and has been measured with the pump–probe method [52,53]. In the simulation, the values of the carrier lifetime were selected to be 100 ps at 10 GHz and 70 ps at 20 GHz in accordance to the theoretical and experimental data provided for the type of SOA that was used in the experiment. The decrease of the carrier lifetime at the higher repetition frequency as used in the model is a result of the higher current at which the SOA has to be driven [53,54] to account for twice the number of pulses entering the amplifier. The carrier lifetime is a particularly important parameter because it defines the range of repetition frequencies at which the ring laser may be operated for a given SOA, as it will be discussed with the simulation results at 20 GHz.

Fig. 5(a) shows the variation of the pulse width, T_{FWHM}, and the normalized energy, U_0, of the mode-locked pulse as well as of the required external pulse energy, α, against the normalized small signal gain coefficient, g_{ss}, at 10 GHz. This figure shows that as the normalized small signal gain increases,

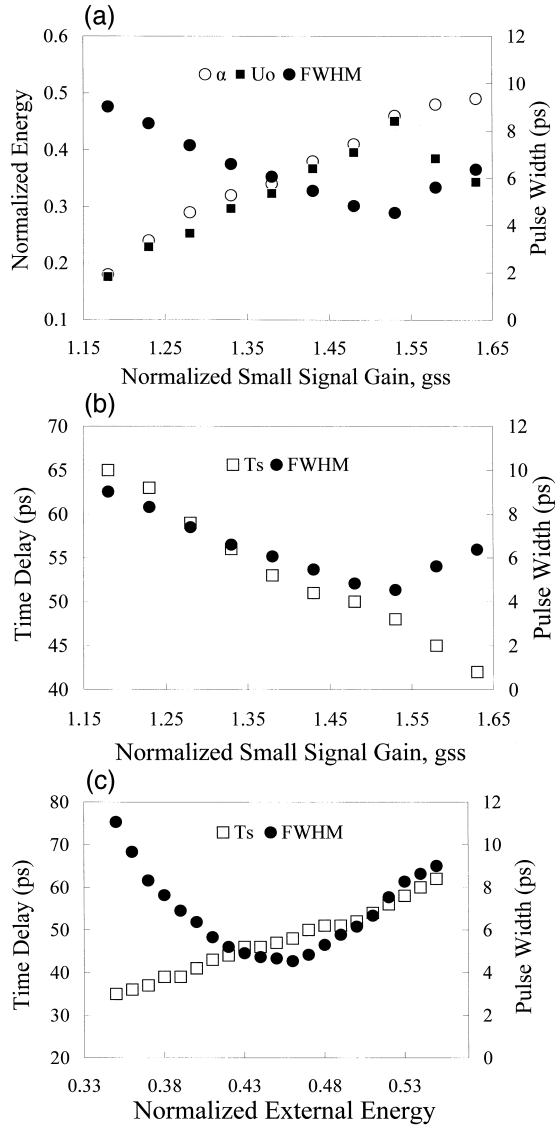

Fig. 5. 10 GHz simulation. (a) Variation of the mode-locked pulse width, FWHM, the normalized energy of the mode-locked pulses, U_0, and external pulses, α, versus the normalized small signal gain, g_{ss}. (b) Variation of the time separation between the mode-locked and external pulses, T_s, versus the normalized small signal gain, g_{ss}. (c) Variation of the time separation between the mode-locked and external pulses, T_s, versus the normalized energy of the external pulses, α.

the energy of the mode-locked pulse also increases saturating the SOA more strongly and leading to pulse narrowing. Similarly, the energy of the external pulse must also be increased to preserve the condition of shortest pulse from the oscillator. The width of the shortest mode-locked pulse decreases up to a minimum value as the normalized gain increases. The minimum pulse width was obtained for 1.53 normalized small signal gain and was 4.5 ps assuming a filter bandwidth of 5 nm in the experimental system. The value of the mode-locked pulse energy, U_0, is either slightly less than or nearly equal to that of the external pulse, α. At the point of minimum pulse width, U_0 takes the value 0.45 and nearly equals α which is 0.46. The SOA is already heavily saturated at the same point and a further increase in the gain beyond this point requires a further increase in the energy of the external pulse, which does not allow an increase in the energy of the mode-locked pulse and results in an increase of its pulse width.

Fig. 5(b) illustrates the variation of the temporal separation, T_s, between the mode-locked and external pulses and for convenience the pulse width, T_{FWHM}, of the mode-locked pulses versus the normalized small signal gain, g_{ss}, at 10 GHz. This figure shows that provided the conditions for best pulse width are maintained, the mode-locked pulse forms at 48 ps, approximately half way between two successive external pulses, despite large variations in g_{ss}. As the small signal gain increases, the mode-locked pulse moves away from the half way point and closer to the leading of the external pulses. The reason for this is that as the small signal gain increases, the gain recovers above the losses in the cavity earlier, forcing the mode-locked pulse to move forward. However, the excess gain increases very gradually so that the mode-locked pulse moves very slowly towards the leading of the two consecutive external pulses.

From the observation and analysis of Fig. 5(a) and (b) it can be deduced that two conditions must be fulfilled in order to obtain mode-locked pulses with the minimum possible width. The first is that the normalized energies of the mode-locked and external pulses must be nearly equal. This condition alone is not sufficient since there is a large set of parameter values for which the normalized energies are equal but the pulse width is not globally minimum as seen in Fig. 5(b). This leads to the second condition which states that the mode-locked pulse must form nearly equidistantly between consecutive external pulses. When both conditions hold, the fiber ring laser system generates the shortest pulses. Fig. 5(c) displays the variation of the time delay, T_s, between the mode-locked and external pulses against the energy of the external pulse normalized to the saturation energy of the SOA. The results shown are for operation of the laser at 10 GHz with the normalized small signal gain set at 1.53. The figure shows that as the energy of the external pulse increases, the mode-locked pulse becomes increasingly delayed with respect to the leading of the two successive external pulses. This is a consequence of the deeper saturation into which the SOA is brought by the external pulse as its energy increases, which in turn requires a longer recovery time for the gain of the SOA to overcome the cavity losses and allow the mode-locked pulse to form. In the same figure the variation of the pulse width against the normalized external pulse energy has been plotted. As seen, the pulse width reaches a minimum value for $\alpha = 0.46$ and forms roughly half way between two consecutive external pulses. An increase of the external pulse energy beyond this point delays the formation of the mode-locked pulse further and results in its broadening.

The model was next used to evaluate the performance of the laser system as the repetition frequency of the external pulse train was increased to 20 GHz. In order to examine the behavior of the model, initially the same values for the physical parameters were used as in the case for 10 GHz operation. This time, however, the width of the mode-locked pulses was longer than that of the external pulses. Note that an increase in the repetition rate of the oscillator restricts the range of values that T_s may take, so that there is no overlap between the external and mode-locked pulses. The parameter that most critically determines the quality of mode-locking, however, is the carrier lifetime of the SOA. If the recovery time is far too short for a given repetition period, the gain of the SOA recovers too fast so that the mode-locked pulse forms early behind the external pulse. This allows the development of excess gain at its trailing edge, resulting in longer mode-locked pulses. On the contrary, if the recovery time is far too long, the

mode-locked pulse trails too far behind the external pulse and has insufficient energy to strongly modulate the gain of the SOA, being therefore long again. In order to obtain a rule of thumb for the carrier lifetime, the theory of standard mode-locking is considered which stipulates that mode-locked pulses form in a laser cavity if the normalized gain function $g(t)$ is greater than 1 just as the pulse forms. In all other instances, that is ahead and behind the pulse, $g(t)$ must be smaller than 1. In this sense and so as to ensure pulse formation, the carrier lifetime must be selected so that

$$g_{\mathrm{in}}^{\mathrm{p}} > 1 \tag{32}$$

and

$$g_{\mathrm{f}}^{\mathrm{p}} < 1 \tag{33}$$

Applying first and second-order Taylor expansion approximations in (19) and (22), these conditions provide, respectively,

$$g_{\mathrm{ss}}\frac{y^2}{2} - \left[g_{\mathrm{ss}}(\alpha+1)+1\right]y + g_{\mathrm{ss}}\frac{\alpha^2}{2} - U_0 - \alpha > 0 \tag{34}$$

and

$$g_{\mathrm{ss}}(1-U_0)\frac{y^2}{2} - \left[g_{\mathrm{ss}}(1-U_0)(\alpha+1)+1\right]y + g_{\mathrm{ss}}(1-U_0)\frac{\alpha^2}{2} - U_0 - \alpha < 0 \tag{35}$$

where $y = -(T_{\mathrm{R}} - 2t_{\mathrm{ext}}/t_{\mathrm{car}})$. For a mode-locked pulse to form, these inequalities must hold simultaneously which happens if

$$1.1(T_{\mathrm{R}} - 2t_{\mathrm{ext}}) < t_{\mathrm{car}} < 2.1(T_{\mathrm{R}} - 2t_{\mathrm{ext}}) \tag{36}$$

which sets a lower and an upper limit for the amplifier carrier lifetime with respect to the repetition period and the width of the external pulse. This condition implies that for the mode-locked pulses to form, the carrier lifetime of the SOA must decrease as the operating frequency of the ring laser increases. The inverse relationship between the carrier lifetime and the operating frequency may be explained if the roles of the frequency and small signal gain in the mode-locking process are considered. Specifically, an increase of the operating frequency requires an increase of the small signal gain in order to compensate the decrease in energy of the mode-locked pulses due to the larger number of pulses entering the amplifier per unit time. Experimentally, an increase of the small signal gain of the SOA is achieved with a higher drive current which also results in a decrease of its carrier lifetime [53,54]. Following the preceding analysis, the carrier lifetime used in the 20 GHz simulation was set to 70 ps. Note that beyond 20 GHz, the carrier lifetime determined by Eqs. (34) and (35) becomes very short and cannot be provided from real SOA devices. This essentially implies that in order to obtain experimentally mode-locked pulses at rates higher than 20 GHz, the laser source must exploit fractional [37,38], instead of conventional, harmonic mode-locking.

Fig. 6(a) depicts the variation of the pulse width and the normalized energy of the mode-locked and external pulses as the normalized small signal gain coefficient is varied at 20 GHz. The behavior of the oscillator is very similar to that presented in Fig. 5(a) for the 10 GHz case. The minimum pulse width obtained was 3.9 ps for an increased normalized small signal gain of 1.83. Despite the increase in the small signal gain, the energies of the mode-locked and external pulses were lower than the 10 GHz case, due to the heavy saturation of the SOA, but were again nearly equal at the point of minimum pulse width ($U_0 = 0.36,\ \alpha = 0.37$). Note that if the same value of small signal gain as for the 10 GHz operation is used, the mode-locked pulses are longer, 7 ps, with lower energy, $U_0 = 0.22$.

Fig. 6(b) shows the variation of the time separation between the mode-locked and external pulses, T_{s}, versus g_{ss}. The pulse width of the mode-locked pulses is also included so as to compare with the results from Fig. 5(b). The variation of the position of the mode-locked pulse at 20 GHz has similar behavior as at 10 GHz, that is, as the small signal gain increases, the mode-locked pulse moves forward towards the leading external pulse. The minimum pulse width is obtained for $T_{\mathrm{s}} = 25$ ps, half way between two consecutive external pulses.

The comparison between the experimental results presented in Section 2 with the results of the theoretical model reveals a very good qualitative agreement between them. In order to assess the ability of the model for quantitative prediction, the parameter values from the experimental set up were substituted in

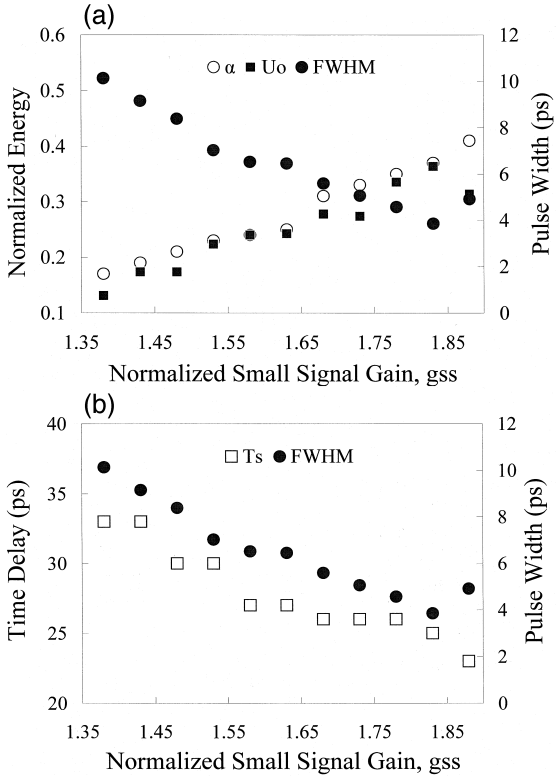

Fig. 6. 20 GHz simulation. (a) Variation of the mode-locked pulse width, FWHM, the normalized energy of the mode-locked pulses, U_0, and external pulses, α, versus the normalized small signal gain, g_{ss}. (b) Variation of the time separation between the mode-locked and external pulses, T_s, versus the normalized small signal gain, g_{ss}.

Eqs. (22), (26)–(28). At 10 GHz, with an experimental value for g_{ss} equal to 1.53 and using a filter of 5 nm spectral bandwidth and external modulating pulses of 8 ps width, the model predicts mode-locked pulses of 4.5 ps duration with normalized energy 0.45 and external pulses with normalized energy 0.46. In this instance the mode-locked pulse forms 48 ps behind the external pulse. At 20 GHz, for an increased normalized gain of 1.78, the model predicts mode-locked pulses of 4.5 ps duration and 0.34 normalized energy forming 26 ps behind the external pulses of 0.35 normalized energy. Experimentally, the shortest pulse train had 4.3 ps duration and formed 49 ps behind the external pulses at 10 GHz. At 20 GHz, the corresponding values were again 4.3 ps and 24 ps delay behind the external pulses.

The qualitative agreement between the experimental and the theoretical values for the pulse width and the relative delay is exceptionally good given the simplicity of the model and suggests its robustness to the approximations that necessarily had to be made. The normalized energy values cannot be effectively compared because the model treats gain, linear loss and filtering of the pulse homogeneously and provides an average cavity value. By comparison, the experimental system has pulse energy values discrete and significantly different in various parts of the cavity.

Finally, in order to assess the dependence of the duration of the output mode-locked pulses on the width of the external pulses, the model ran at 10 GHz and 20 GHz for g_{ss} 1.53 and 1.78, respectively, and for different values of t_{ext}. The obtained results indicate that there is a weak sensitivity of the width of the mode-locked pulses on the width of the external pulses since a 50% change of t_{ext} causes only a 5% change of t_p. This was also observed experimentally.

4.3. Discussion of the mode-locking process

The basic mechanism for mode-locking in the oscillator relies on the periodic, fast saturation of the gain coefficient of the SOA as a result of the introduction of the external pulse train and the subsequent slow gain recovery. The mode-locked pulse forms after the external pulse at the time that the slowly recovering gain of the SOA balances the cavity losses. As the mode-locked pulse transits the SOA, its gain depletes again below the loss line, to recover slowly before the next external pulse enters it. This mode-locking mechanism results in the temporal displacement between the external and mode-locked pulses in the SOA and is depicted in Fig. 7. The parameters that are crucial in the formation of the mode-locked pulse for any repetition frequency are the small signal gain and carrier lifetime of the SOA, the cavity loss and the energy of the external pulse. As already discussed in 4.2, in order to obtain the shortest pulses, these parameters must be adjusted so that the mode-locked pulse forms approximately half way between two consecutive external pulses. This condition is important to be satisfied because it

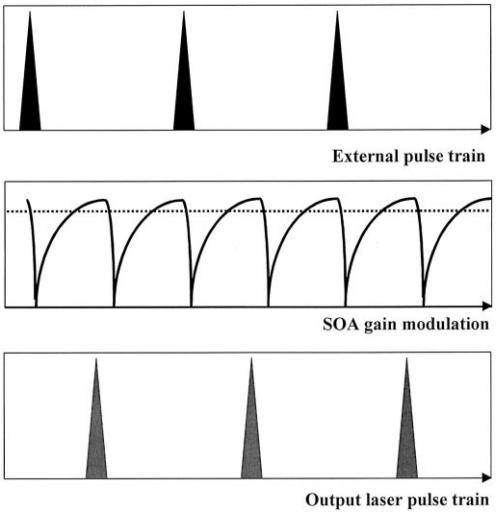

Fig. 7. Mode-locking process based on SOA gain modulation by an external pulse. The dots in the SOA gain modulation curve indicate the loss line above which the net gain is positive enabling the formation of mode-locked pulses.

allows the maximum energy to be extracted from the mode-locked pulse, which in turn locally saturates the SOA more strongly, allowing higher compression of the mode-locked pulse. At the same time, as the mode-locked pulse is responsible for creating the gain modulation function around it in a similar way to passive mode-locking, this mode-locking technique is robust to a wide range of parameters and allows a wide flexibility in the operating conditions of the oscillator. The simple theoretical model that has been described provides a good design tool for the optimum performance of the mode-locked oscillator.

5. Conclusion

We have presented an experimental and a theoretical study of the performance of a short pulse, high repetition rate ring laser source. The source exploits the fast saturation of a semiconductor optical amplifier, forming the gain element in its cavity, from an external optical pulse to generate picosecond pulses. The source has been shown to generate 4.3 ps nearly transform-limited pulses across 16 nm tuning range at 10 and 20 GHz. It has also been shown to be stable against environmental perturbations and it is very simple to build from commercially available components. In order to explain the operation of the source, a complete and computationally simple physical model of the fiber ring laser has been developed to provide solutions for the steady-state mode-locked pulse profile in terms of the critical parameters of the system. This model can predict the duration of the output mode-locked pulses versus the duration of the external pulses. The theoretical as well as the experimental results indicate that the minimum pulse width is obtained when these parameters are adjusted so that the mode-locked pulse forms midway between two successive external pulses and that this condition corresponds to the case where the energies of the external and mode-locked pulses are nearly equal. Since the laser is expected to find application as a high repetition rate source for transmission or optical logic experiments, a practical rule of thumb has been derived for the required carrier lifetime of the SOA, for the source to operate at any given repetition frequency. The direct comparison of the experimental and theoretical results has revealed an excellent agreement between them and has helped to provide a thorough explanation of the mode-locking process.

Acknowledgements

The authors would like to thank G. Guekos, R. Dall'Ara and H. Burkhard for providing the SOA and DFB laser devices and LYCOM for the dispersion compensating fiber. This work was partially supported by the CEC via the ESPRIT program, project 36078, DO_ALL. K. Zoiros gratefully acknowledges financial support from GSRT and INTRACOM, Greece.

References

[1] E.A. Swanson, S.R. Chinn, K.L. Hall, K.A. Rauschenbach, R.S. Bondurant, J.W. Miller, IEEE Photon. Technol. Lett. 6 (1994) 1194.
[2] S. Kawanishi, H. Takara, K. Uchiyama, I. Shake, K. Mori, Electron. Lett. 35 (1999) 826.
[3] K.L. Hall, K.A. Rauschenbach, Opt. Lett. 23 (1998) 1271.
[4] T.J. Xia, Y. Liang, K.H. Ahn, J.W. Lou, O. Boyraz, Y.H. Kao, X.D. Cao, S. Chaikamnerd, J.K. Andersen, M.N. Islam, IEEE Photon. Technol. Lett. 10 (1998) 153.

[5] K. Zoiros, T. Houbavlis, K. Vlachos, H. Avramopoulos, F. Girardin, G. Guekos, S. Hansmann, H. Burkhard, CLEO Tech. Dig. CThF5 (1999) 379.
[6] J.D. Kafka, T. Bauer, D.W. Hall, Opt. Lett. 14 (1989) 1269.
[7] A. Takada, H. Miyazawa, Electron. Lett. 26 (1990) 216.
[8] D. Jones, H. Haus, E. Ippen, Opt. Lett. 21 (1996) 1818.
[9] T.F. Carruthers, I.N. Duling III, Opt. Lett. 21 (1996) 1927.
[10] H. Takara, S. Kawanishi, M. Saruwatari, K. Noguchi, Electron. Lett. 28 (1992) 2095.
[11] T. Pfeiffer, G. Veith, Electron. Lett. 29 (1993) 1849.
[12] E. Yoshida, Y. Kimura, M. Nakazawa, Electron. Lett. 31 (1995) 377.
[13] G.T. Harvey, L.F. Mollenauer, Opt. Lett. 18 (1993) 107.
[14] X. Shan, D.M. Spirit, Electron. Lett. 29 (1993) 979.
[15] C.R. Doerr, H.A. Haus, E.P. Ippen, M. Shirasaki, K. Tamura, Opt. Lett. 19 (1994) 31.
[16] J.S. Wey, J. Goldhar, D.W. Rush, M.W. Chbat, G.M. Carter, G.L. Burdge, IEEE Photon. Technol. Lett. 7 (1995) 152.
[17] M.J. Guy, J.R. Taylor, D.G. Moodie, A.E. Kelly, Electron. Lett. 32 (1996) 2240.
[18] K. Sato, I. Kotaka, Y. Kondo, M. Yamamoto, Appl. Phys. Lett. 69 (1996) 2626.
[19] H. Porte, T. Frison, P. Mollier, J.P. Goedgebuer, IEEE Photon. Technol. Lett. 7 (1995) 700.
[20] T. Papakyriakopoulos, A. Stavdas, E.M. Protonotarios, H. Avramopoulos, Electron. Lett. 35 (1999) 717.
[21] K.Y. Lau, A. Yariv, Appl. Phys. Lett. 46 (1985) 326.
[22] G. Eisenstein, R.S. Tucker, S.K. Korotky, U. Koren, R.M. Jopson, L.W. Stulz, J.J. Veselka, K.L. Hall, Electron. Lett. 21 (1985) 173.
[23] G. Eisenstein, R.S. Tucker, U. Koren, S.K. Korotky, IEEE J. Quantum Electron. 22 (1986) 142.
[24] S.W. Corzine, J.E. Bowers, G. Przybylek, U. Koren, B.I. Miller, C.E. Soccolich, Appl. Phys. Lett. 52 (1988) 348.
[25] R.S. Tucker, U. Koren, G. Raybon, C.A. Burrus, B.I. Miller, T.L. Koch, G. Eisenstein, Electron. Lett. 25 (1989) 621.
[26] G. Raybon, P.B. Hansen, R.C. Alferness, L.L. Buhl, U. Koren, B.I. Miller, M.G. Young, T.L. Koch, J.-M. Verdiell, C.A. Burrus, Opt. Lett. 18 (1993) 1335.
[27] N.V. Pedersen, K.B. Jakobsen, M. Vaa, J. Lightwave Technol. 14 (1996) 833.
[28] H. Shi, J. Finlay, G.A. Alphonse, J.C. Conolly, P.J. Delfyett, IEEE Photon. Technol. Lett. 9 (1997) 1439.
[29] H. Shi, G.A. Alphonse, J.C. Conolly, P.J. Delfyett, Electron. Lett. 34 (1998) 179.
[30] C. Schmidt, E. Dietrich, S. Diez, H.J. Ehrke, U. Feiste, L. Kuller, R. Ludwig, H.G. Weber, CLEO Tech. Dig. CThA3 (1999) 348.
[31] D.M. Patrick, Electron. Lett. 30 (1994) 43.
[32] K.L. Hall, J.D. Moores, K.A. Rauschenbach, W.S. Wong, E.P. Ippen, H.A. Haus, IEEE Photon. Technol. Lett. 7 (1995) 1093.
[33] T. Papakyriakopoulos, A. Hatziefremidis, T. Houbavlis, H. Avramopoulos, OFC Tech. Dig. TuB1 (1999) 4.
[34] X. Wang, H. Yokoyama, T. Shimizu, IEEE Photon. Technol. Lett. 8 (1996) 617.
[35] J.D. Moores, W.S. Wong, K.L. Hall, Opt. Lett. 20 (1995) 2547.
[36] N. Onodera, A.J. Lowery, L. Zhai, Z. Ahmed, R.S. Tucker, Appl. Phys. Lett. 62 (1993) 1329.
[37] T. Papakyriakopoulos, K. Vlachos, A. Hatziefremidis, H. Avramopoulos, Opt. Lett. 24 (1999) 717.
[38] K. Vlachos, K. Zoiros, T. Houbavlis, A. Hatziefremidis, H. Avramopoulos, LEOS Proc. ThN1 (1999) 768.
[39] D.J. Kuizenga, A.E. Siegman, IEEE J. Quantum Electron. 6 (1970) 694.
[40] G.H.C. New, IEEE J. Quantum Electron. 10 (1974) 115.
[41] H.A. Haus, IEEE J. Quantum Electron. 11 (1975) 736.
[42] H.A. Haus, Jpn. J. Appl. Phys. 20 (1981) 1007.
[43] L.A. Zenteno, H. Avramopoulos, G.H.C. New, Appl. Phys. B 40 (1986) 141.
[44] H.A. Haus, J. Appl. Phys. 51 (1980) 4042.
[45] J.A. Yeung, IEEE J. Quantum Electron. 17 (1981) 399.
[46] M. Schell, A.G. Weber, E.H. Boettcher, E. Scholl, D. Bimberg, IEEE J. Quantum Electron. 27 (1991) 402.
[47] J.E. Bowers, P.A. Morton, A. Mar, S.W. Corzine, IEEE J. Quantum Electron. 25 (1989) 1426.
[48] R.J. Helkey, P.A. Morton, J.E. Bowers, Opt. Lett. 15 (1990) 112.
[49] M. Schell, A.G. Weber, E. Scholl, D. Bimberg, IEEE J. Quantum Electron. 27 (1991) 1661.
[50] P.J. Delfyett, A. Dienes, J.P. Heritage, M.Y. Hong, Y.H. Chang, Appl. Phys. B 58 (1994) 183.
[51] G. Agrawal, N.A. Olsson, IEEE J. Quantum Electron. 25 (1989) 2297.
[52] K.L. Hall, G. Lenz, A.M. Darwish, E.P. Ippen, Opt. Commun. 111 (1994) 589.
[53] F. Girardin, G. Guekos, A. Houbavlis, IEEE Photon. Technol. Lett. 10 (1998) 784.
[54] G. Eisenstein, R.S. Tucker, J.M. Wiesenfeld, P.B. Hansen, G. Raybon, B.C. Johnson, T.J. Bridges, F.G. Storz, C.A. Burrus, Appl. Phys. Lett. 54 (1989) 454.